Available online at www.sciencedirect.com
ScienceDirect
Trans. Nonferrous Met. Soc. China 29(2019) 964−975
Transactions of Nonferrous Metals Society of China
www.tnmsc.cn

Effect of reverse dual rotation process on properties of friction stir welding of AA7075 to AISI304

Hamed JAMSHIDI AVAL[1], Altino LOUREIRO[2]

1. Department of Materials Engineering, Babol Noshirvani University of Technology, Shariati Avenue, Babol, Iran;
2. CEMUC, Department of Mechanical Engineering, University of Coimbra, Rua Luís Reis Santos, 3030-788 Coimbra, Portugal

Received 4 July 2018; accepted 7 November 2018

Abstract: The friction stir lap welding of AISI304 stainless steel to AA7075 aluminium alloy was investigated using the conventional friction stir welding (C-FSW) and the reverse dual rotation friction stir welding (DR-FSW) processes. In order to reduce the heat input, a dual rotation tool with a lower shoulder rotating speed was used. The results showed that both processes provide welds with excellent appearance and free of internal defects. The use of the DR-FSW process with the tool shoulder rotating reversely at low speed results in larger grain refinement in the nugget and less change in the microstructure of the aluminium alloy than using the C-FSW. The use of DR-FSW process at low speed of rotation allows to reduce the amount of intermetallic compounds in the welding interface, but does not prevent their formation. Although DR-FSW welding exhibits tensile strength superior to that achieved with the conventional process (C-FSW), both exhibit brittle behaviour with fracture at the weld interface.
Key words: dual rotation tool; dissimilar friction stir welding; AA7075; AISI304; microstructure; mechanical properties

1 Introduction

The establishment of aluminium to steel bonding has a high potential for industrial use because it allows the combination of low density and good corrosion resistance of aluminium with the high rigidity and mechanical strength of the steel. The automotive industry has great interest not only in the use of these joints, because it allows to reduce the weight of the vehicles and consequently the consumption of fuel, but also for complex applications in the aerospace industry [1]. Since fusion welding processes are not used in the establishment of such bonds, because of the large melting temperature difference and the strong tendency to form brittle intermetallic compound (IMC) [2], other processes such as mechanical joining, adhesive bonding or solid state welding have been tempted. The mechanical bonds are expensive, not tight and in some cases it is difficult to control the plastic deformation of high strength aluminium and high strength steels [3]. On the other hand, the adhesive bonded joints are sensitive to extreme environmental conditions and age [4], besides the requirements of surface treatment and joint geometry. Solid state welding process such as explosive welding [5] or friction stir welding [6] has been used in Al−Fe joints but brittle IMCs such as Al_5Fe_2, FeAl and $FeAl_3$ were found at the weld interface. The formation of these IMCs can be prevented or decreased by decreasing the interaction between Al and Fe, as ZHENG et al [6] did, introducing a Zn foil between aluminium and steel in FSW in overlapping joints. As the formation of intermetallic is a thermally activated process, another way to lessen the formation of IMCs is to reduce the heat input in the process.

In conventional friction stir welding (FSW), the speed gradient between pin centre and the maximum diameter of the shoulder may result in thermal softening of the weld region or incipient melting of certain heat-treatable aluminium alloys [7]. To avoid this problem, the dual-rotation FSW [8] and reverse dual-rotation FSW [7,9] were proposed as a variant technique. Dual-rotation technique allows the relative rotational speeds of the probe and the shoulder to be varied. In other words,

Corresponding author: Hamed JAMSHIDI AVAL; Tel: +98-11-35501808; Fax: +98-11-35501802; E-mail: h.jamshidi@nit.ac.ir
DOI: 10.1016/S1003-6326(19)65005-3

an optimized combination of rotational speeds for both probe and shoulder can be selected. It is called non-rotational shoulder-assisted FSW (NRSA-FSW) [10] when the rotation speed of assisted shoulder is zero. However, it can be divided into the co-rotating dual-rotation FSW (CDR-FSW) [11] and the reverse dual-rotation friction stir welding (RDR-FSW) [7] when the rotation speed of assisted shoulder is not zero. LI and LIU [7,9,11] studied the reverse dual-rotation friction stir welding of aluminium alloy 2219-T6. They showed that RDR-FSW results in improving the joint property by adjusting heat generation through separately designed tool shoulder and tool pin. Furthermore, they reported that the coarsening and dissolution degrees of precipitates in the weld nugget zone (WNZ), shoulder affected zone (SAZ), thermo-mechanically affected zone (TMAZ), and heat-affected zone (HAZ) of RDR-FSW joint were much smaller, as compared with the conventional FSW joint. LI and LIU [12] examined the effect of non-rotational shoulder (NRS) tool in friction stir welding of aluminium alloy 2219-T6. They found that at a constant welding speed of 100 mm/min, defect-free joints can only be obtained at a tool rotation speed of 800 r/min by the FSW, without assistance of the NRS. However, the NRSA-FSW can produce defect-free joints in a wider range of tool rotation speeds of 600−900 r/min. Moreover, they reported that the maximum tensile strength of NRSA-FSW joints is 69% of the base material. However, that of conventional FSW is 71.2% of the base material. SHI et al [13−15] studied the material flow and heat transfer in reversal dual rotation of 2024 aluminium alloy using a 3D CFD model. They reported that the reverse material flow due to reverse rotation of tool probe and shoulder, is beneficial to the uniform distribution of both the temperature and microstructure on the advancing and retreating sides of the welds.

The FSW has been widely reported on joining aluminium alloy and steel. OGURA et al [16] studied the mechanical properties and interfacial microstructure of a friction stir welded AA3003 aluminium alloy/AISI304 stainless steel dissimilar lap joint. They reported that the strength in the centre region and on the advancing side was larger than that at the retreating side. FEREIDUNI et al [17] examined the effect of welding parameters on the joint interface microstructure and shear strength of friction stir spot welded AA5083/St12 alloy sheets. They found that the formation of a relatively thick intermetallic layer at the joint interface as well as the grain growth of aluminium at the exit hole periphery decrease tensile shear strength of joints. HUANG et al [18,19] investigated microstructure and material flow in self-riveting friction stir lap welding of AA6082 aluminium alloy to QSTE340TM steel. They reported that the synergistic effect of mechanical bonding induced by the riveting and metallurgical bonding induced by the Al/Fe intermetallic layer contributed to high strength of the self-riveting friction stir lap welding joint. SHAMSUJJOHA et al [20] studied the effects of plunge depth, bonding area, and top sheet positions on the microstructure and mechanical properties of dissimilar FSW of 1018 mild steel and AA6061. They reported that a joint efficiency of 58% was achieved when right handed lap welds were made using the pin tool with longer pin length. MAHTO et al [21] examined mechanical properties and microstructural evolutions in friction stir lap welding of AAA6061 and AISI304. They found that the fracture occurred outside the weld region, which indicated that a thinner intermetallic compound did not have a detrimental effect on the weld strength. HATANO et al [22] studied the relationship between intermetallic compound layer thickness with interfacial strength for dissimilar joints of AAA6061 and AISI304. They demonstrated that the fracture position can be determined by the percentage of the joining area via the intermetallic layer thickness below a threshold value, which was 0.4 μm.

According to literature, dual rotation tool is a suitable candidate to avoid over-thermal softening of the weld region or formation of thick intermetallic compounds in the dissimilar joint of aluminium and steel alloys. Up to date, the effect of dual rotation tool on the mechanical and microstructural behaviours in friction stir lap welding of AISI304 stainless steel to AA7075 aluminium alloy has less been investigated. In the present work, an attempt has been made to understand the effects of reverse dual rotation tool on microstructures and mechanical properties during the friction stir lap welding of AA7075-T6 and AISI 304 stainless steel. This was done through comparing it with the conventional FSW joint. Accordingly, microstructural evolution and mechanical properties were studied utilizing optical and transmission electron microscope and tensile testing.

2 Experimental

The high-strength aluminium alloy 7075-T6 (5.21 Zn, 2.30 Mg, 1.32 Cu, 0.10 Mn, 0.21 Si, 0.37 Fe, Al balance, in wt.%) with the thickness of 2 mm and 1 mm-thick 304 austenite stainless steel (18.50 Cr, 8.10 Ni, 0.44 Cu, 1.20 Mn, 0.05 C, Fe balance, in wt.%) were chosen as the base materials. Plates of dimensions 200 mm × 100 mm were machined and used for welding. The single-pass friction stir lap welds were conducted using a friction stir welding machine. Shear overlap joints were formed so that the overlap length was 50 mm. Transverse joints were formed on the overlapping sheets.

The FSW tool was applied on the aluminium side, because according to AKBARI et al [23] in dissimilar lap welding of Al to Cu the best results are obtained by welding from the Al side. It should be noted that the position control method with 0.2 mm plunge depth was employed in the welding experiments. Two tools, conventional and dual rotating (DR)-FSW, with the inclination angle of 2.5° were used in this study. For conventional FSW tool, a rotational speed of 1000 r/min and a traverse speed of 120 mm/min were employed in welding operations. For DR-FSW tool, a traverse speed of 120 mm/min and pin and shoulder rotational speed of 1000 and 600 r/min were employed, respectively. The shoulder rotational speed was decreased in order to reduce further the heat input in the process [24]. The DR-FSW tool system is composed of the tool pin, rotating with the spindle of the FSW machine during the welding process, and the surrounding assisted shoulder, rotating reversely by using driving gears mounted on the tool box. Figure 1 shows DR-FSW tool used in this study. Both tools have 14 mm in diameter shoulder with 2° conical cavity and a cylindrical pin measuring 5 mm in diameter and 2.1 mm in length. The AA7075-T6 aluminium alloy was located in the advancing side, whereas AISI304 was positioned in the retreating side. Hereafter, the joints made by dual rotating and conventional FSW tool were referred as DR-FSW and C-FSW, respectively. The temperature profiles were in situ measured using the K-type thermocouples with a 0.25 mm-in-diameter wire. Two thermocouples were inserted at the advancing side and retreating side at a distance of 3 mm from the weld line.

The cross sections of the joints were used for metallographic analysis and mechanical tests. The cross sections were polished using diamond pastes and etched with a reagent made of 3 mL nitric acid (HNO_3), 6 mL hydrofluoric acid (HF), 6 mL hydrochloric acid (HCl), and 150 mL H_2O. Microstructural analysis was carried out using transmission electron microscopy (TEM) and an optical microscope, incorporated with image analysing software (Clemex–Vision). The grain sizes were determined based on ASTM E112 and the general intercept procedure. Microhardness profiles were measured on the polished cross sections with a test load of 1 N for 15 s. Tensile shear specimens were removed transversely to the welding direction, prepared according to ASTM D1002 standard and tested in tension with a constant cross head speed of 1 mm/min.

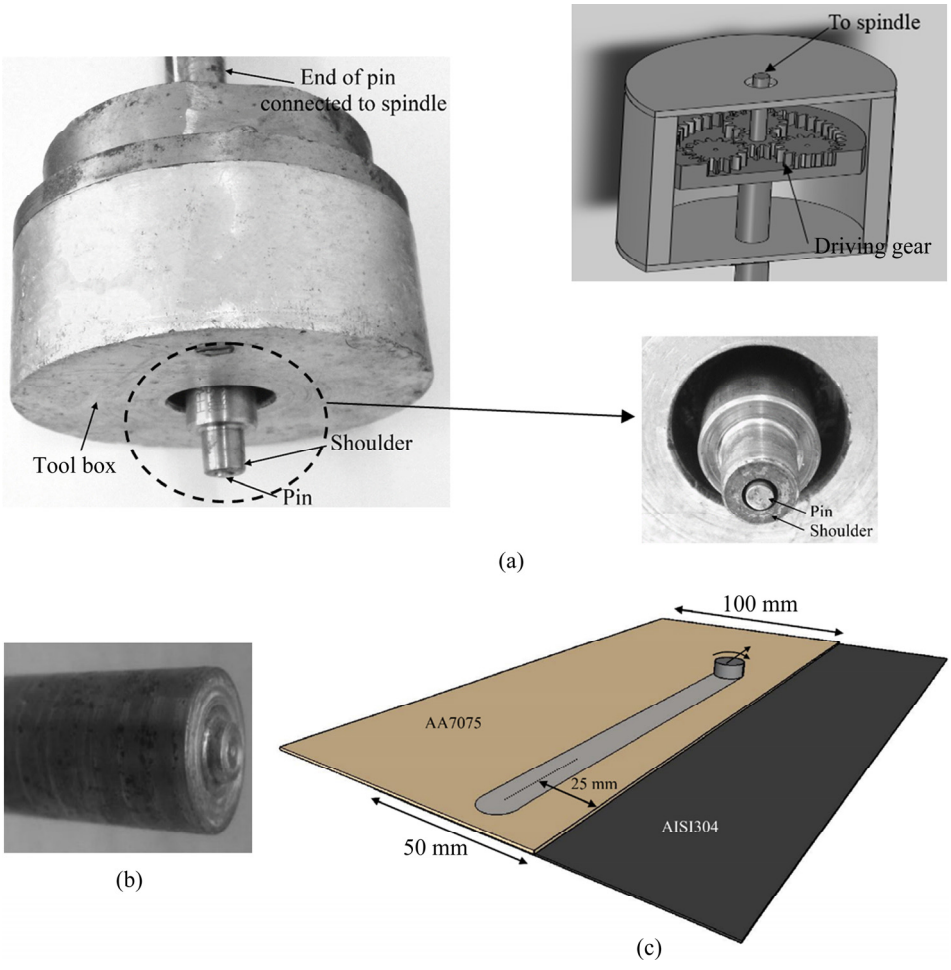

Fig. 1 Tools and joint design used in this study: (a) DR-FSW; (b) Conventional FSW; (c) Joint design and welding sample dimension

3 Results and discussion

3.1 Weld morphology

Figure 2 shows the crowns of the welded samples with little flash formed on both sides of the weld line in any of the weld series. The crown of the C-FSW joint shows smooth striations due to the higher rotation speed of the tool shoulder, with the spacing between striations of 0.12 mm (120/1000) for C-FSW and 0.20 mm (120/600) for DR-FSW. According to KRISHNAN [25], striation spacing is proportional to the traverse/rotational speed ratio and to the forward motion of the tool in one rotation. With decreasing the traverse/rotational speed ratio, the striation spacing is decreased and the weld surface is smoother.

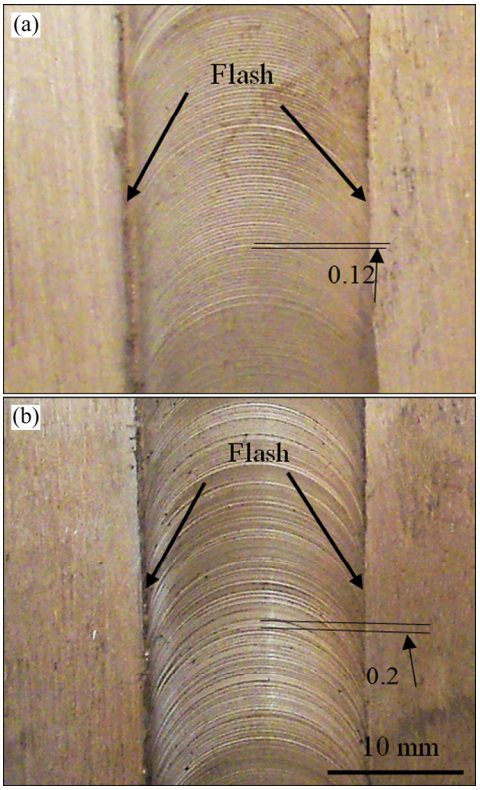

Fig. 2 Crowns of welded samples: (a) Made by C-FSW tool; (b) Made by DR-FSW tool

The transverse cross-section of joints made by DR-FSW and C-FSW is shown in Fig. 3. In both welds, inserting the rotating pin in the stainless steel causes the flow of the steel workpiece upwards and causes an effect similar to hooking. The presence of hook reduces the effective thickness of the top plate and hence load bearing area of top plate, during tensile shear testing, resulting in lower tensile shear strength. The hook size does insert a deep effect through stress concentration during loading [26]. Although the rotational speed of the pin is equal in both the samples, the height of steel part flow in the joint made by DR-FSW is much lower. The steel maximum fragment height in the joint made by DR-FSW and C-FSW is 0.45 and 0.71 mm, respectively. In other words, the higher speed of the tool shoulder produces more heat. This results in easier flowing of the bottom workpiece in the weld nugget and higher amount of steel fragments in the joint made by C-FSW. The higher steel fragment height or lower steel fragment angle means a reduction in the effective thickness of the aluminium workpiece, which has a great effect on the joint strength and decreases the load carrying capacity [27]. Another important point is the orientation of the hooks around the weld nugget. The hooks' direction is influenced by the upward flow of material and the sidewise flow induced by the rotating shoulder. The upward and to the inside orientation of the steel fragments in the weld nugget of DR-FSW indicates the stronger and more dominant upward flow. The reverse and lower rotation speed of the tool's shoulder decreased the sideward flow of steel fragment. In the joint made by C-FSW, higher material shearing due to higher rotational speed of shoulder forced the material sideward and reduced the hook curvature. The fact that the shoulder rotation is opposite to the pin rotation in the case of the DR-FSW process can also contribute to the increased angles referred to. In any case, it can be concluded that it is possible to achieve the welds with any of the process variants.

3.2 Weld microstructure

Compared with the joint welded by the conventional FSW, the weld zones in the DR-FSW joint are similar and can be divided into the weld nugget zone (WNZ), the thermo-mechanically affected zone (TMAZ), the heat affected zone (HAZ) and base material (BM). The different weld zones and microstructure of WNZ in the aluminium and steel part are shown in Figs. 3 and 4, respectively. Grain size in stainless steel and aluminium alloy base metals was (52±3) and (48±5) μm (Figs. 4(a) and 4(b)). Similar to the previous researches, the nugget region consisted of equiaxed grains (Figs. 4(c−f)). The dynamic recrystallization mechanism in steel and aluminium was different due to the difference in the staking fault energy (SFE) [28]. However, the recrystallized grains were observed on both sides of the aluminium and steel in the WNZ. This microstructure represented the occurrence of dynamic recrystallization in this region [29,30]. The heat input has a significant effect on the recrystallization at the stir zone [31]. The grain growth is prominent at high temperature, which results in increased grain size as heat input increases. The recrystallized grain size on the aluminium side of WNZ in the joint made by C-FSW and DR-FSW is (8.3±0.2) and (5.2±0.3) μm, respectively. The grain size in the

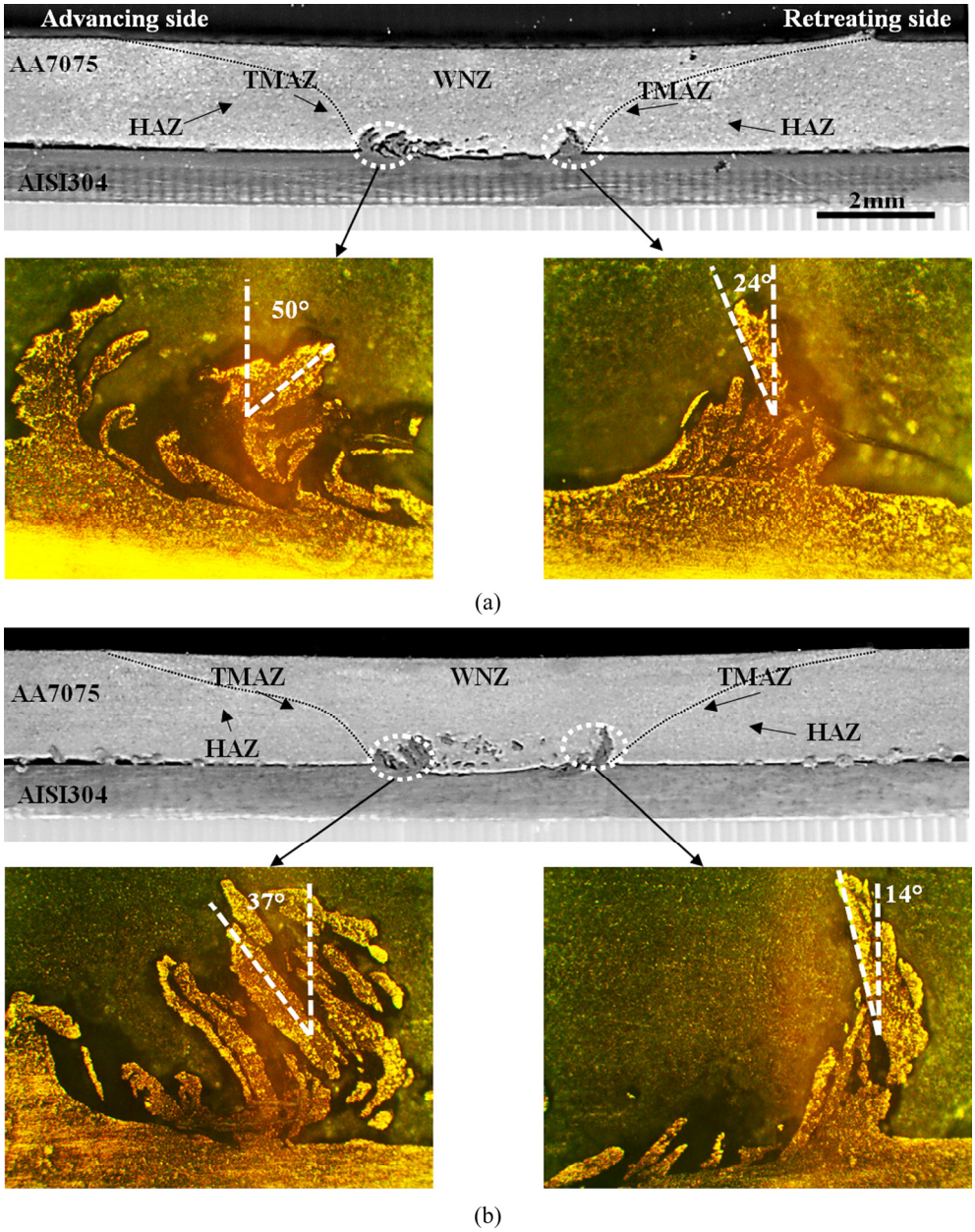

Fig. 3 Macrostructures of welded sample: (a) DR-FSW; (b) C-FSW

WNZ of DR-FSW sample is finer than that in the joint made by C-FSW (Figs. 4(e) and (f)), which suggests lower heat input and lower driving force for the grain growth in the joint made by DR-FSW. It is noteworthy that most changes in the WNZ grain size are seen on the aluminium side and there is no appreciable difference inthe grain size on the steel side (Figs. 4(c) and (d)). The recrystallized grain size on the steel side of WNZ in the joint made by C-FSW and DR-FSW is (5.3±0.4) and (4.8±0.3) μm, respectively, confirming the earlier observation of lower heat generated in the DR-FSW process.

Figure 5 shows SEM images of joint interface of the welded samples. According to the EDS results of the various points, the analyses of points A and B in both samples were related to steel and aluminium base metals, respectively. According to the chemical composition of the steel fragment interface with aluminium matrix (point C), this point contained 45 at.% Al and 40 at.% Fe, which suggests the likelihood for the formation of intermetallic compounds (IMCs) close to the FeAl. SEM/EDS analysis showed that the interconnection and thickness of these IMCs in this sample are far greater for C-FSW welds than for DR-FSW. In addition to steel fragments, alumina and iron-rich compounds are also observed in the aluminium matrix of both welds, as shown in Fig. 5.

The mechanical properties of age-hardening aluminium alloys strongly depended on the type, morphology, and distribution of precipitates. In the

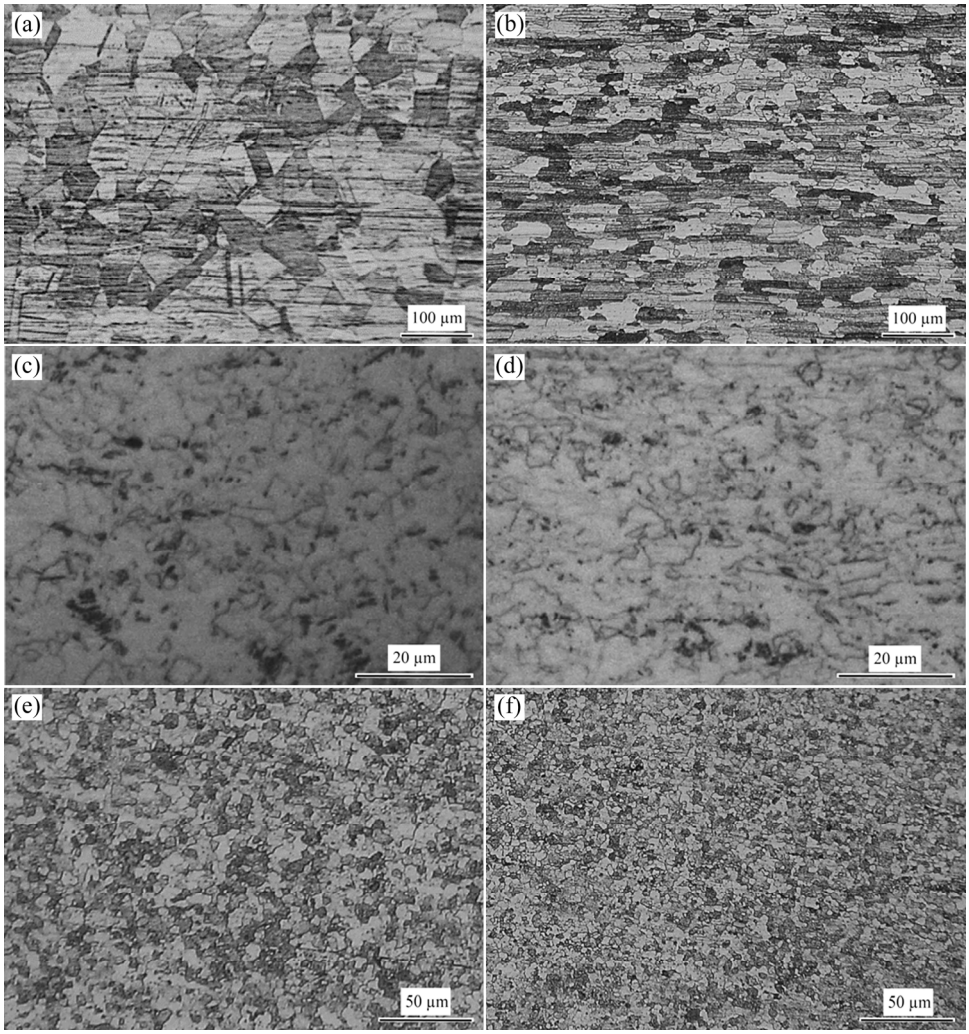

Fig. 4 Optical metallography images: (a) Base metal of AISI 304; (b) Base metal of AA7075; (c) WNZ at AISI 304 side of sample C-FSW; (d) WNZ at AISI 304 side of sample DR-FSW; (e) WNZ at AA7075 side of sample C-FSW; (f) WNZ at AA707 side of sample DR-FSW

Al−Zn−Mg−(Cu) system (7xxx alloys) with Mg-to-Zn ratio lower than 0.5, the precipitation sequence was generally reported as SS → GP zones (MgZn) → η' → η($MgZn_2$) [32]. Most of the strength was associated with the precipitation of GP zones and η' semi-coherent phases. Losses in strength could be found due to dissolution, coarsening or over ageing of the precipitates in the 7xxx alloys. Due to small differences in size between aluminium and solute in AA7075, spherical GP zones were formed [33], whereas the η' phase presents as round or plate shape particles. The η phase precipitated in various shapes such as plates, rods and laths, depending on the orientation relationship [34]. Figures 6(a) and (b) show that the TEM microstructure of AA7075-T6 base metal contained very small (4−8 and 10−80 nm) precipitates and low dislocation density. SU et al [35] and FULLER et al [36] showed that η' and η were coarser precipitates and the GP zones were the smaller ones. The HAZ of both DR-FSW and C-FSW showed dissolution and coarsening of strengthening precipitates (Figs. 6(c) and (d)). Moreover, the precipitate free zone (PFZ) (due to grain boundaries) acting as sinks for vacancies as well as heterogeneous nucleation sites could be seen in the HAZ. Compared to HAZ of C-FSW joint, finer precipitates with higher density and narrower PFZ were formed in the HAZ of DR-FSW joint. This was due to lower heat generation and temperature in the HAZ of DR-FSW joint which result in decreasing diffusion rate. The TMAZ of joints, either DR-FSW or C-FSW, contained low-angle grain boundary, cellular recovery structures, and dislocation (Figs. 6(e) and (f)). The heat and plastic deformation during FSW changed size, type and distribution of precipitates. The precipitates coarsening due to more heat generation was more visible in the TMAZ of C-FSW joint. According to temperature measurement in TMAZ of both the joints, the peak temperatures in TMAZ of DR-FSW and C-FSW were 380 and 415 °C, respectively.

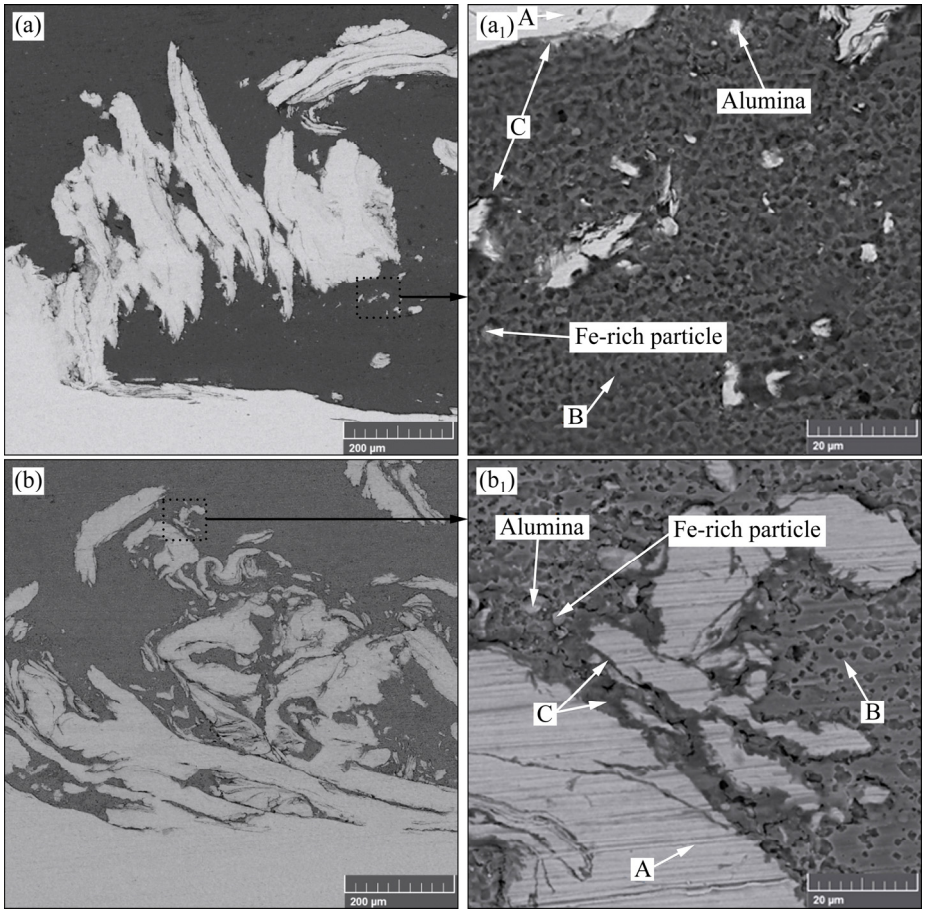

Fig. 5 SEM images of joint interface of welded samples: (a, a_1) DR-FSW; (b, b_1) C-FSW

The peak temperature in the TMAZ was higher than the solution temperature of η' phase [37], which could result in dissolution of the precipitates and heterogeneous distribution. The coarsening of the precipitates is much less and more homogeneous in the DR-FSW joint certainly due to the lower temperatures reached in the process.

Figure 7(a) shows the thermal cycles measured on the feed side of both welds. Also, the density of the dislocations in DR-FSW is much higher compared to the C-FSW joint. The higher temperature, 410 °C in the DR-FSW and 480 °C in the C-FSW joints (see Fig. 7(a)), and sever plastic deformation in the SZ, resulted in more dissolution, coarsening of precipitates, and lower dislocation density, as compared to TMAZ (Figs. 6(g) and (h)). However, higher temperature in the C-FSW led to more dissolution of the existing precipitates and lower dislocation density in the SZ. The higher temperature in the SZ of C-FSW resulted in an extreme change in heating and cooling rate (see Fig. 7(b)). According to Ref. [38], this extreme change produced solid solution in the SZ. Therefore, this zone could respond well to natural aging after welding. In short, the use of the DR-FSW process instead of the C-FSW reduces the heat generated in the process which influences the formation of intermetallic compounds in the weld, refines the grain in the nugget and produces less change in the microstructure of the aluminium alloy.

3.3 Mechanical properties

Figure 8 shows the hardness distribution in the transverse cross-section of the welds. A significant heterogeneity in hardness distribution could be seen among different weld zones. As commonly found in friction stir welding of age-hardening aluminium alloys [39−41], a significant softening took place in the SZ, TMAZ and HAZ, as compared to the aluminium base material. On the other hand, due to strain hardening and dynamic recrystallization in the vicinity of the interface, hardness increased as compared to AISI304 base metal. However, the minimum hardness in the aluminium part of joint C-FSW was lower than that in the DR-FSW joint, 60.4 and 65.1 $HV_{0.1}$ for C-FSW and DR-FSW joint, respectively. As discussed earlier, a higher temperature and more over-aging occurred in the TMAZ, SZ and HAZ of the C-FSW joint result in larger hardness decrease. However, there was not much difference in the hardness of the stainless-steel part in the

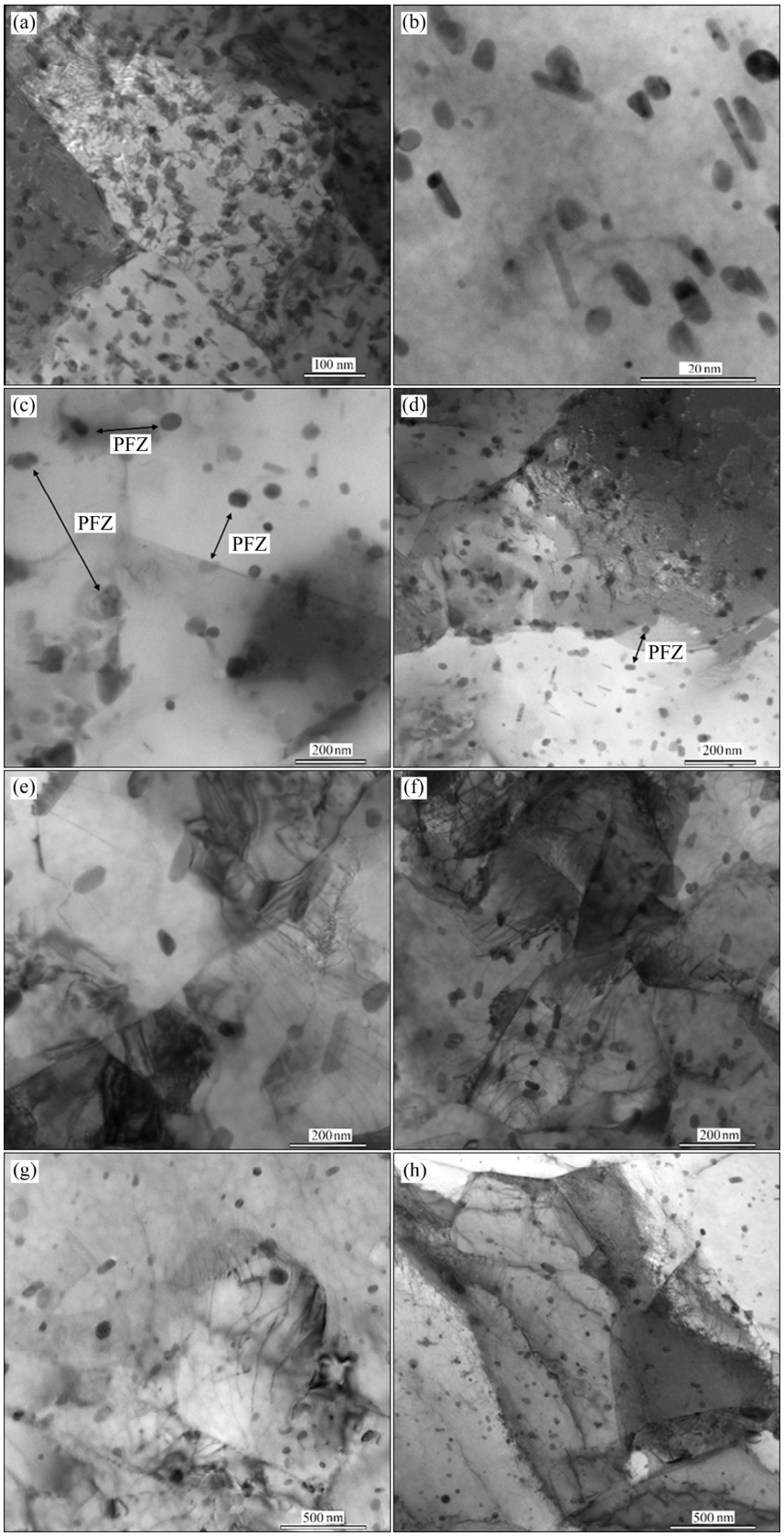

Fig. 6 TEM bright field images of different zones of AA7075 side: (a) Base material of AA7075-T6; (b) Base material of AA7075-T6 with higher magnification; (c) HAZ of joint made by C-FSW tool; (d) HAZ of joint made by DR-FSW tool; (e) TMAZ of joint made by C-FSW tool; (f) TMAZ of joint made by DR-FSW tool; (g) SZ of joint made by DR-FSW tool; (h) SZ of joint made by DR-FSW tool

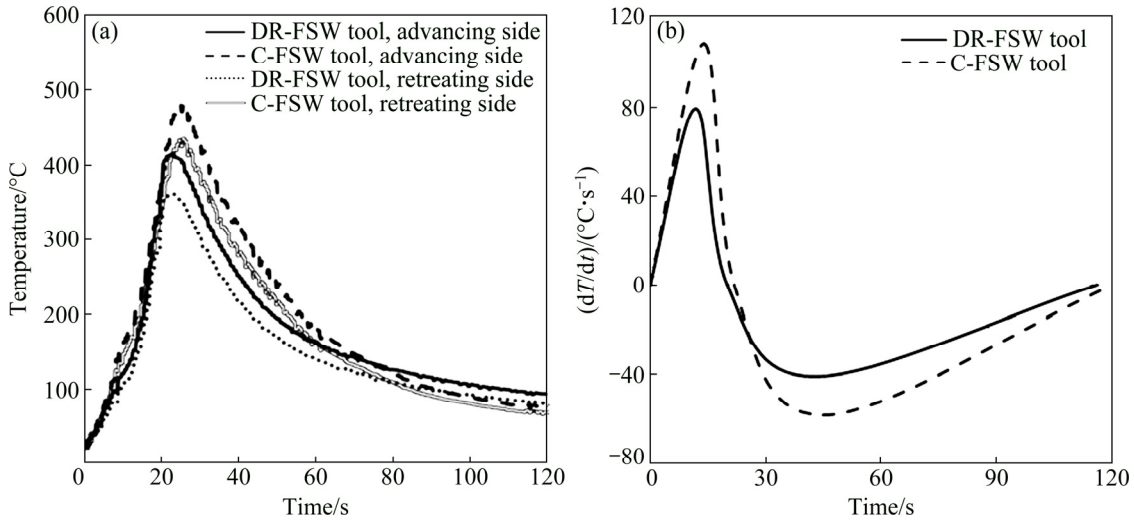

Fig. 7 Measured thermal cycles at 3 mm from weld centre line at advancing and retreating sides (a) and change rate of temperature with respect to time at advancing side (b)

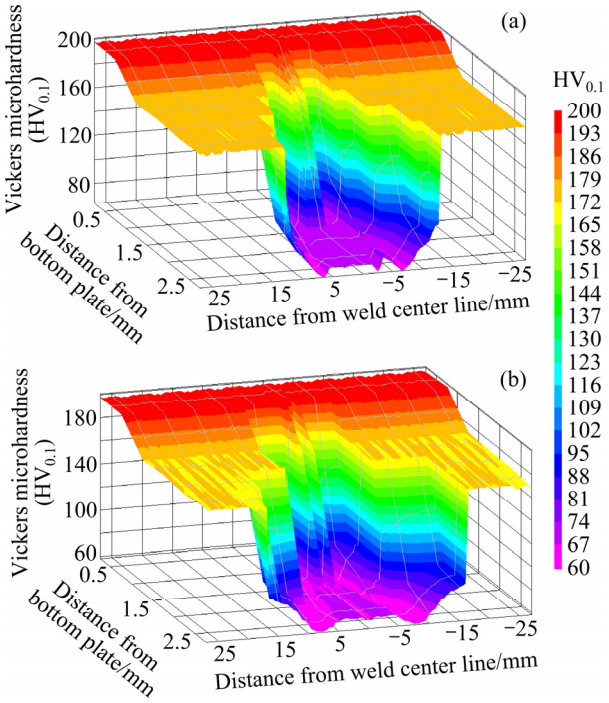

Fig. 8 Microhardness profiles: (a) DR-FSW; (b) C-FSW

vicinity of the interface. The increasing SZ hardness, as compared to TMAZ, could be related to steel pieces and intermetallic compounds formed in this zone. This also stood true for some reprecipitation of strengthening precipitates in this zone. This hardness increase could be seen in the microhardness profile at weld centre line and at a distance of 0−0.5 mm from the upper surface of SS304 base metal, as indicated with arrows in the images.

Examples of the load−displacement curves of welded samples are shown in Fig. 9(a). The mechanical behaviour is similar for both welds; however, the C-FSW welding has lower load and elongation at break than the DR-FSW weld, which suggests better ductility of the latter. In both weld series, the fracture occurred in the interface of the welds. These fractures present brittle character due to the presence of intermetallic compounds.

The XRD spectra obtained on the fracture surfaces of both welds revealed the presence of FeAl intermetallic compound in both welds (see Fig. 10). In the dissimilar joint of aluminium and steel alloys, intermetallic compound is usually generated. When intermetallic compound forms in the joint, it leads to a remarkable decrease in the tensile strength of the joint [42]. In the joint of a solid-state joining process, the formation of the intermetallic compounds can be limited by selecting suitable joining parameters to control the temperature and time in the joint. The joint interface temperature and the thickness of the intermetallic compound at the interface during friction stir welding are decreased with the decrease of welding heat input. This shows that although the DR-FSW process generates less heat in the weld than the C-FSW process, producing smaller structural changes, it had no inhibitory effect on intermetallic compound formation in the joint interface. The maximum load bearing capacity of joint C-FSW was lower than that in the DR-FSW joint, 18 and 20 kN for C-FSW, and DR-FSW joint, respectively. The lower strength of the C-FSW joint can be related mainly to the presence of the hard and brittle intermetallic compound at the weld interface, as observed by WANG et al [43]. This calls into question of the possibility of obtaining Al−steel welds by friction stir welding, resorting only to the reduction of heat-input in the process.

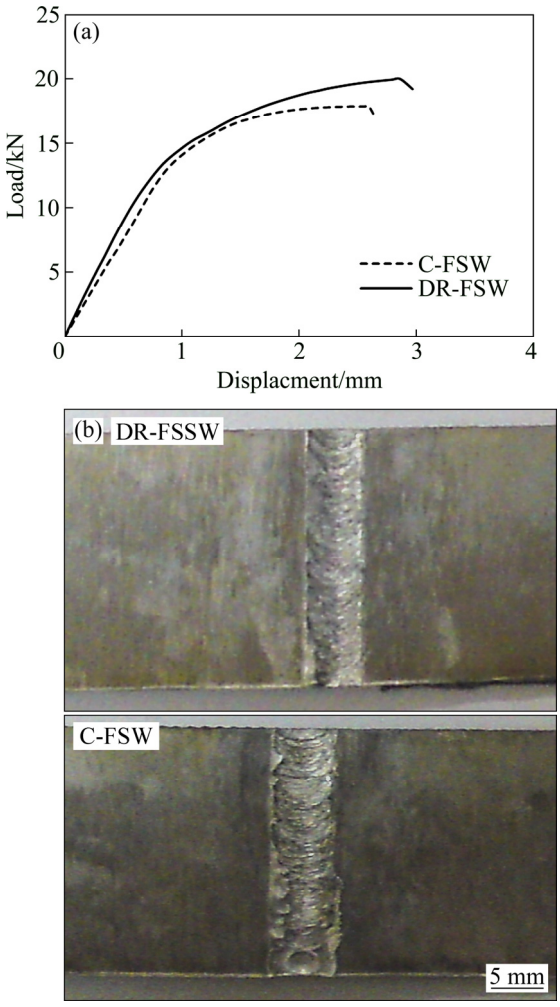

Fig. 9 Load−displacement curve of welded samples (a) and fracture surface at steel side (b)

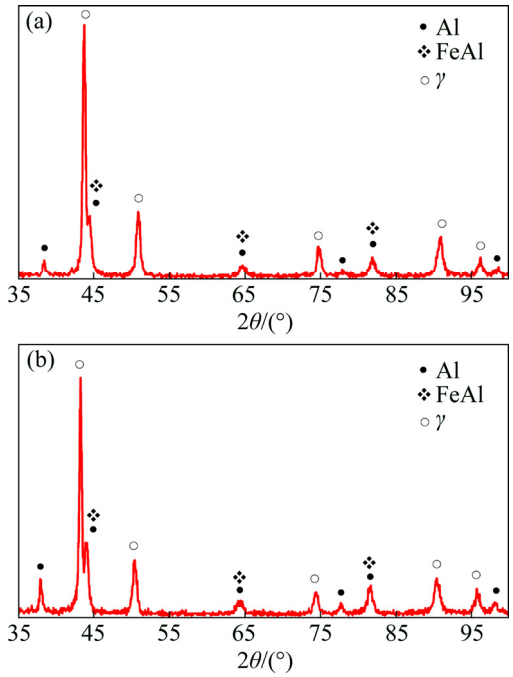

Fig. 10 XRD patterns of fracture surface at steel side of sample: (a) DR-FSW; (b) C-FSW

4 Conclusions

(1) The C-FSW and DR-FSW processes allow the production of dissimilar welds with good surface appearance and free of internal defects.

(2) The higher speed of the tool shoulder produced more heat, which resulted in easier material flow of the bottom workpiece in the weld nugget and higher amount of steel fragments in the joint made by C-FSW. The steel fragment height in the joint made by DR-FSW and C-FSW is 0.45 and 0.71 mm, respectively. The higher curvature of steel part in the joint made by C-FSW tool reduced the effective thickness of the aluminium workpiece and the joint strength. The maximum load bearing capacity of joint C-FSW was lower than that in the DR-FSW joint, 18 and 20 kN for C-FSW and DR-FSW joint, respectively.

(3) Lower heat generation and temperature in the HAZ of the DR-FSW joint result in finer precipitates with higher density and narrower PFZ. Also, the density of dislocations in DR-FSW is much higher compared to the C-FSW joint.

(4) Higher temperature and more over-aging occurred in the TMAZ, SZ and HAZ of joint C-FSW, resulting in lower minimum hardness in the aluminium part of C-FSW joint. The minimum hardness in the aluminium part of joint C-FSW and DR-FSW joint was 60.4 and 65.1 $HV_{0.1}$, respectively.

(5) The reduction of heat generated in the DR-FSW process reduced the amount of intermetallic compounds at the interface but it was not sufficient to ensure good mechanical behaviour of the weld.

Acknowledgments

The first author acknowledges the funding support of Babol Noshirvani University of Technology (No. BNUT/370167/97). Altino LOUREIRO acknowledges the support of programme COMPETE, Programa Operacional Factores de Competitividade, and of FCT-Fundação Portuguesa para a Ciência e a Tecnologia, under the project UID/EMS/00285/2013.

References

[1] SCHUBERT E, KLASSEN M, ZERNER I, WALZ C, SEPOLD G. Light-weight structures produced by laser beam joining for future applications in automobile and aerospace industry [J]. Journal of Materials Processing Technology, 2001, 115(1): 2−8.

[2] SUN Jun-hao, YAN Qi, GAO Wei, HUANG Jian. Investigation of laser welding on butt joints of Al/steel dissimilar materials [J]. Materials and Design, 2015, 83: 120−128.

[3] MORI K I, ABE Y. A review on mechanical joining of aluminium and high strength steel sheets by plastic deformation [J]. International Journal of Lightweight Materials and Manufacture, 2018, 1(1): 1−11.

[4] SU Ning, MACKIE R I, HARVEY W J. The effects of ageing and environment on the fatigue life of adhesive joints [J]. International Journal of Adhesion and Adhesives, 1992, 12(2): 85−93.

[5] CARVALHO G H S F L, GALVÃO I, MENDES R, LEAL R M, LOUREIRO A. Formation of intermetallic structures at the interface of steel-to-aluminium explosive welds [J]. Materials Characterization, 2018, 142: 432−442.

[6] ZHENG Q, FENG X, SHEN Y, HUANG G, ZHAO P. Dissimilar friction stir welding of 6061Al to 316 stainless steel using Zn as a filler metal [J]. Journal of Alloys and Compounds, 2016, 686: 693−701.

[7] LI J Q, LIU H J. Characteristics of the reverse dual-rotation friction stir welding conducted on 2219-T6 aluminum alloy [J]. Materials and Design, 2013, 45: 148−154.

[8] THOMAS W M, KALLEE S W, STAINES D G, OAKLEY P J. Friction stir welding – Process developments and variant techniques [C]//SAE World Congress 2006. Cobo Center, Detroit, Michigan, 2006: 1−8.

[9] LI J Q, LIU H J. Optimization of welding parameters for the reverse dual-rotation friction stir welding of a high-strength aluminum alloy 2219-T6 [J]. The International Journal of Advanced Manufacturing Technology, 2015, 76(5): 1469−1478.

[10] LI J Q, LIU H J. Design of tool system for the external nonrotational shoulder assisted friction stir welding and its experimental validations on 2219-T6 aluminum alloy [J]. The International Journal of Advanced Manufacturing Technology, 2013, 66(6): 623−634.

[11] LI J Q, LIU H J. Effects of the reversely rotating assisted shoulder on microstructures during the reverse dual-rotation friction stir welding [J]. Journal of Materials Science & Technology, 2015, 31(4): 375−383.

[12] LI J Q, LIU H J. Design of tool system for the external nonrotational shoulder assisted friction stir welding and its experimental validations on 2219-T6 aluminum alloy [J]. The International Journal of Advanced Manufacturing Technology, 2013 66(5): 623−634.

[13] SHI L, WU C S, LIU H J. Modeling the material flow and heat transfer in reverse dual-rotation friction stir welding [J]. Journal of Materials Engineering and Performance, 2014, 23(8): 2918−2929.

[14] SHI L, WU C S, LIU H J. Numerical analysis of heat generation and temperature field in reverse dual-rotation friction stir welding [J]. The International Journal of Advanced Manufacturing Technology, 2014, 74(1): 319−334.

[15] SHI L, WU C S, LIU H J. Analysis of heat transfer and material flow in reverse dual-rotation friction stir welding [J]. Welding in the World, 2015, 59(5): 629−638.

[16] OGURA T, SAITO Y, NISHIDA T, NISHIDA H, YOSHIDA T, OMICHI N, FUJIMOTO M, HIROSE A. Partitioning evaluation of mechanical properties and the interfacial microstructure in a friction stir welded aluminum alloy/stainless steel lap joint [J]. Scripta Materialia, 2012, 66(8): 531−534.

[17] FEREIDUNI E, MOVAHEDI M, KOKABI A H. Aluminum/steel joints made by an alternative friction stir spot welding process [J]. Journal of Materials Processing Technology, 2015, 224: 1−10.

[18] HUANG Yong-xian, HUANG Ti-fang, WAN Long, MENG Xiang-chen, ZHOU Li. Material flow and mechanical properties of aluminum-to-steel self-riveting friction stir lap joints [J]. Journal of Materials Processing Technology, 2019, 263: 129−137.

[19] HUANG Yong-xian, WANG Ji-chao, WAN Long, MENG Xiang-chen, LIU Hong-bing, LI Hao. Self-riveting friction stir lap welding of aluminum alloy to steel [J]. Materials Letters, 2016, 185: 181−184.

[20] SHAMSUJJOHA M, JASTHI B K, WEST M, WIDENER C. Friction stir lap welding of aluminum to steel using refractory metal pin tools [J]. Journal of Engineering Materials and Technology, 2015, 137(2): 021009.

[21] MAHTO R P, KUMAR R, PAL S K, PANDA S K. A comprehensive study on force, temperature, mechanical properties and micro-structural characterizations in friction stir lap welding of dissimilar materials (AA6061-T6 & AISI304) [J]. Journal of Manufacturing Processes, 2018, 31: 624−639.

[22] HATANO R, OGURA T, MATSUDA T, SANO T, HIROSE A. Relationship between intermetallic compound layer thickness with deviation and interfacial strength for dissimilar joints of aluminum alloy and stainless steel [J]. Materials Science and Engineering A, 2018, 735: 361−366.

[23] AKBARI M, ABDI BEHNAGH R, DADVAND A. Effect of materials position on friction stir lap welding of Al to Cu [J]. Science and Technology of Welding and Joining, 2012, 17(7): 581−588.

[24] COLEGROVE P A, SHERCLIFF H R, ZETTLER R. Model for predicting heat generation and temperature in friction stir welding from the material properties [J]. Science and Technology of Welding and Joining, 2007, 12(4): 284−297.

[25] KRISHNAN K N. On the formation of onion rings in friction stir welds [J]. Materials Science and Engineering A, 2002, 327: 246−251.

[26] YUE Yu-mei, ZHOU Zhen-lu, JI Shu-de, ZHANG Jin, LI Zheng-wei. Effect of welding speed on joint feature and mechanical properties of friction stir lap welding assisted by external stationary shoulders [J]. The International Journal of Advanced Manufacturing Technology, 2017, 89(5): 1691−1698.

[27] WANG T, SIDHAR H, MISHRA R S, HOVANSKI Y, UPADHYAY P, CARLSON B. Friction stir scribe welding technique for dissimilar joining of aluminium and galvanised steel [J]. Science and Technology of Welding and Joining, 2018, 23(3): 249−255.

[28] SAKAI T, BELYAKOV A, KAIBYSHEV R, MIURA H, JONAS J J. Dynamic and post-dynamic recrystallization under hot, cold and severe plastic deformation conditions [J]. Progress in Materials Science, 2014, 60: 130−207.

[29] PATEL V V, BADHEKA V, KUMAR A. Influence of friction stir processed parameters on superplasticity of Al−Zn−Mg−Cu alloy [J]. Materials and Manufacturing Processes, 2016, 31(12): 1573−1582.

[30] PATEL V V, BADHEKA V, KUMAR A. Effect of polygonal pin profiles on friction stir processed superplasticity of AA7075 alloy [J]. Journal of Materials Processing Technology, 2017, 240: 68−76.

[31] PATEL V V, BADHEKA V, KUMAR A. Friction stir processing as a novel technique to achieve superplasticity in aluminum alloys: Process variables, variants, and applications [J]. Metallography, Microstructure, and Analysis, 2016, 5(4): 278−293.

[32] LORIMER G W, NICHOLSON R. Further results on the nucleation of precipitates in the Al−Zn−Mg system [J]. Acta Metallurgica, 1966, 14: 1009−1013.

[33] TOTTEN G E, MACKENZIE D S. Handbook of aluminum: Physical metallurgy and processes [M]. New York: CRC Press, 2003.

[34] DEGISCHER H P, LACOM W, ZAHRA A, ZAHRA C Y. Decomposition processes in an Al−5%Zn−1%Mg alloy. II. Electronmicroscopic investigations [J]. Zeitschrift fur Metallkunde, 1980, 71: 231−238.

[35] SU J Q, NELSON T W, MISHRA R, MAHONEY M. Microstructural investigation of friction stir welded 7050-T651 aluminium [J]. Acta Materialia, 2003, 51: 713−729.

[36] FULLER C B, MAHONEY M W, CALABRESE M, MICONA L. Evolution of microstructure and mechanical properties in naturally aged 7050 and 7075 Al friction stir welds [J]. Materials Science and Engineering A, 2010, 527: 2233−2240.

[37] ZHOU L, WANG T, ZHOU W L, LI Z Y, HUANG Y X, FENG J C. Microstructural characteristics and mechanical properties of 7050-T7451 aluminum alloy friction Stir-Welded Joints [J]. Journal of Materials Engineering and Performance, 2016, 25(6): 2542−2550.

[38] MARTINEZ N, KUMAR N, MISHRA R S, DOHERTY K J. Microstructural variation due to heat gradient of a thick friction stir

welded aluminum 7449 alloy [J]. Journal of Alloys and Compounds, 2017, 713: 51−63.

[39] MARTINEZ N, KUMAR N, MISHRA R S, DOHERTY K J. Effect of tool dimensions and parameters on the microstructure of friction stir welded aluminum 7449 alloy of various thicknesses [J]. Materials Science and Engineering A, 2017, 684: 470−479.

[40] LEITAO C, ARRUTI E, ALDANONDO E, RODRIGUES D M. Aluminium−steel lap joining by multipass friction stir welding [J]. Materials and Design, 2016, 106: 153−160.

[41] JAMSHIDIAVAL H. Microstructure and residual stress distributions in friction stir welding of dissimilar aluminium alloys [J]. Materials and Design, 2015, 87: 405−413.

[42] KIMAPONG K, WATANABE T. Effect of welding process parameters on mechanical property of FSW lap joint between aluminum alloy and steel [J]. Materials Transactions, 2005, 46(10): 2211−2217.

[43] WANG Qian, LENG Xue-song, YANG Tian-hao, YAN Jiu-chun. Effects of Fe−Al intermetallic compounds on interfacial bonding of clad materials [J]. Transactions of Nonferrous Metals Society of China, 2014, 24(1): 279−284.

逆向差速搅拌摩擦焊对 AA7075 与 AISI304 焊缝性能的影响

Hamed JAMSHIDI AVAL[1], Altino LOUREIRO[2]

1. Department of Materials Engineering, Babol Noshirvani University of Technology, Shariati Avenue, Babol, Iran;

2. CEMUC, Department of Mechanical Engineering, University of Coimbra, Rua Luís Reis Santos, 3030-788 Coimbra, Portugal

摘　要：对比研究传统搅拌摩擦焊(C-FSW)和逆向差速搅拌摩擦焊(DR-FSW)两种工艺搭焊 AISI304 不锈钢和 AA7075 铝合金的性能。为了减少热输入，采用低轴肩转速的双旋转搅拌头。研究结果表明，采用两种工艺均能获得外观优良、无内部缺陷的焊缝。与 C-FSW 相比，采用轴肩低速逆向旋转的 DR-FSW 工艺可使熔核晶粒细化程度提高，且铝合金组织变化较小。使用低速旋转的 DR-FSW 不能阻止焊接界面中金属间化合物的形成，但可以减少其数量。与采用传统工艺(C-FSW)相比，采用 DR-FSW 工艺获得的焊缝具有更高的抗拉强度，两者的焊接界面均表现出脆性断裂行为。

关键词：双旋转搅拌头；异种搅拌摩擦焊；AA7075；AISI304；显微组织；力学性能

(Edited by Bing YANG)